Draft version February 5, 2008
Preprint typeset using LaTeX style emulateapj

QUASAR EVOLUTION AND THE BALDWIN EFFECT IN THE LARGE BRIGHT QUASAR SURVEY

Paul J. Green, Karl Forster, & Joanna Kuraszkiewicz
Harvard-Smithsonian Center for Astrophysics, 60 Garden St., Cambridge, MA 02138
email: *pgreen@cfa.harvard.edu, kforster@cfa.harvard.edu, jkuraszkiewicz@cfa.harvard.edu*

Draft version February 5, 2008

ABSTRACT

From a large homogeneous sample of optical/UV emission line measurements for 993 quasars from the Large Bright Quasar Survey (LBQS), we study correlations between emission line equivalent width and both restframe ultraviolet luminosity (i.e., the Baldwin Effect) and redshift. Our semi-automated spectral fitting accounts for absorption lines, fits blended iron emission, and provides upper limits to weak emission lines. Use of a single large, well-defined sample and consistent emission line measurements allows us to sensitively detect many correlations, most of which have been previously noted. A new finding is a significant Baldwin Effect in UV iron emission. Further analysis reveals that the primary correlation of iron emission strength is probably with redshift, implying an evolutionary rather than a luminosity effect. We show that for most emission lines with a significant Baldwin Effect, and for some without, evolution dominates over luminosity effects. This may reflect evolution in abundances, in cloud covering factors, or overall cloud conditions such as density and ionization. We find that in our sample, a putative correlation between Baldwin Effect slope and the ionization potential is not significant. Uniform measurements of other large quasar samples will extend the luminosity and redshift range of such spectral studies and provide even stronger tests of spectral evolution.

Subject headings: galaxies: active — quasars: emission lines — quasars: general — ultraviolet: galaxies

1. INTRODUCTION

Because the simplest photoionization models for the emission-line regions of quasars predict a linear proportionality between line and continuum strength, diagnostics such as equivalent widths (the ratio of integrated line flux over local continuum flux density) would be expected naively to be *independent* of continuum luminosity. Baldwin (1977) first noticed that the CIV λ1549Å emission line equivalent width (W_λ hereafter) in quasars *decreases* with increasing UV continuum (1450Å) luminosity. Since flux *ratios* like W_λ are distance-independent, this discovery brought hope that, regardless of its physical explanation, the ensemble Baldwin Effect (EBEff hereafter) might enable quasars (QSOs) to be used as a "standard candle" in measuring cosmological distances.

Unfortunately, the large dispersion in this anticorrelation (e.g., Baldwin, Wampler, & Gaskell 1989; Zamorani et al. 1992) yields poor distance calibrations relative to other standard candles. Relative luminosity distances accurate to 10% at $z \sim 0.5$ and 20% at $z = 1$ are becoming possible with Type Ia supernova measurements (e.g., Garnavich et al. 1998; Perlmutter et al. 1999). Combining these results with those of Boomerang, COBE, Planck, and MAP should more tightly constrain cosmological models in the near future (Park et al. 1998; Melchiorri 2000). A deeper understanding of the EBEff, elusive though it still seems, is worth pursuing for several reasons. First, QSOs represent the most distant non-transient bright objects observable in the Universe, extending to $z \sim 6$ (Fan et al. 2000). Second, substantial reduction in the scatter is not critical to use of the EBEff for cosmology. A 'main sequence fitting' approach with an ensemble of quasars could yield useful cosmological constraints, as long as we can be confident that there are no significant unaccounted for evolutionary effects (Baldwin 1999). Third, the EBEff harbors some important information on the nature and evolution of QSOs themselves. If we can understand both the origin of the EBEff and the source(s) of scatter, we will have learned much about the intrinsic physics of QSOs.

Physical processes or variables that could dominate the EBEff were recently sketched by Sergeev et al. (1999) and Green (1999), and include (1) Geometry - The inclination of an accretion disk could change the apparent continuum luminosity alone (Wilkes et al. 1999; Netzer, Laor, & Gondhalekar 1992). (2) Covering factor - A decrease in covering factor of broad emission line (BEL) clouds with luminosity (Wu, Boggess, & Gull 1983). (3) Optically thin clouds - As the dominant ionization state of the element changes, a flat or even *negative* correlation between continuum flux and line emission for a given species can result (Shields, Ferland & Peterson 1995). (4) Changes in spectral energy distribution (SED) with luminosity - A softer ionizing continuum in more luminous nuclei (Green 1998; Korista et al. 1998; Wandel 1999a) causes a decrease in emission line flux.

Observationally, a significant EBEff has been claimed not only for CIV, but also for ions such as OVI, He II, CIII], Mg II, and Lyα (e.g., Tytler & Fan 1992; Zamorani et al. 1992). In all cases, we refer to slopes in the log-log domain of equivalent width W_λ vs. luminosity L. Thus, a slope β_w describes $W_\lambda \propto L^{\beta_w}$. Typical slopes [1] for CIV are $\beta_w \sim -0.2$ (Kinney, Rivolo, & Koratkar 1990) and

[1]Some studies characterize the relationships as $W_\lambda \propto M_V^{\beta_m}$ ($\beta_m = -0.4\beta_w$; Zamorani et al. 1992; Zheng, Fang, & Binette 1992), or $L_{line} \propto L^\beta$ ($\beta = 1 + \beta_w$; Pogge & Peterson 1992).

there have been claims that the EBEff shows steeper slopes for lines of higher ionization energy (Zheng, Fang, & Binette 1992; Espey & Andreadis 1999). In the SED picture, steeper slopes are naturally expected for species of higher ionization energy, since shifts in the relative normalization between their driving and underlying (UV) continuum are then more effective. An observational effect that has yet to be fully accounted for is that the narrow component of emission lines varies most with luminosity in samples of QSOs (Osmer, Porter, & Green 1994).

A line/continuum anticorrelation analogous to the EBEff is also observed in multi-epoch optical/UV spectroscopy of individual active galactic nuclei (AGN) of lower luminosity ($M_B > -23$). The steep slope of the intrinsic Baldwin effect (IBEff) ($\beta_w \sim -0.7$) may add considerable scatter to the shallower EBEff, ($\beta_w \sim -0.2$; both slopes from Kinney, Rivolo, & Koratkar 1990), unless suitably time-averaged data are used for every object. The scatter in the IBEff decreases once time lags between emission line and continuum variations are removed (Pogge & Peterson 1992). The IBEff appears to persist even into the hard X-ray regime (for the Fe Kα emission line; Iwasawa & Taniguchi 1993; Reeves et al. 2001). While multi-epoch spectroscopy and time-lag correction for large AGN samples might reduce scatter, practically speaking, it is prohibitive. Furthermore, variability anticorrelates with luminosity in AGN (Helfand et al. 2001; Webb & Malkan 2000; Giveon et al. 1999), so that scatter from the IBEff is unlikely to dominate in high luminosity QSOs.

Unfortunately, many studies of the EBEff have been conducted using compilations of measurements from the literature. These compilations mix samples that are diverse in their selection criteria, in the resolution and quality of their spectra, and in the techniques used to measure them. Line measurement techniques for large samples suffer from difficulty in achieving consistent and reliable measurements of the continuum, and of blended line emission. The latter problem is particularly thorny for the blended iron multiplets (FeI, FeII, and FeIII) and emission lines in close proximity. [2] Absorption within the line profiles is rarely accounted for, and while few studies provide upper limits to undetected emission lines, the latter are invaluable for confirming or constraining claimed trends. We have therefore undertaken a major study of quasar line emission, accounting for absorption lines and blended iron emission, using largely automated procedures on carefully-selected samples, and providing upper limits for undetected lines. The analysis of samples of QSOs with more than a few hundred spectra requires some amount of automatization to give consistent results. The largest sample of QSO spectra currently available is that of the Large Bright Quasar Survey. Forster et al. (2001; Paper I hereafter) describe the initial results from emission line measurements of 993 LBQS QSOs (excluding those with strong broad absorption). Here, we use these measurements to study the Baldwin effect in the LBQS.

2. SIGNIFICANT LUMINOSITY CORRELATIONS

Here we describe correlations between W_λ and the rest-frame UV luminosity. We use L_{2500}, the monochromatic luminosity at 2500Å obtained by extrapolating B_J photometric magnitude and assuming a continuum slope of $\alpha = 0.5$ ($f_\nu \sim \nu^\alpha$). Photometric magnitudes are superior to those estimated from the spectra themselves, since the LBQS spectra are not spectrophotometric. Use of luminosities calculated for other rest wavelengths would simply offset the $\log L_{2500}$ value for each quasar by a fixed amount (e.g., 26% fainter at λ1549, 43% fainter at λ1216), whereas we concern ourselves with EBEff slopes. Optical luminosities are calculated assuming $H_0 = 50$ km s^{-1} Mpc^{-1}, $q_0 = 0.5$, and $\Lambda = 0$, with further details in Green et al. (1995).

The W_λ values and corresponding errors that we use are from Paper I, but in cases where emission lines were modeled by more than one Gaussian component (exclusively for strong lines like Lyα, C IV, and Mg II), we have combined those measurements, yielding a single W_λ measurement for all objects. The median per-pixel signal-to-noise ratio (S/N) of the LBQS spectra is typically ∼5, independent of redshift. Our emission line fitting procedure yields uncertainty estimates, all of which are available in Paper I. The resulting emission line S/N can be characterized by ratio of the W_λ values to their $1-\sigma$ errors. Representative median (mean) S/N for strong UV line measurements are 5-6 (6-10). Weaker lines (e.g., Hγ, O Iλ1305, O IIλ3728, Si IV+OIV]λ1400) have S/N between 3-5. For emission lines that are not detected, we include 2σ upper limits to W_λ using the survival analysis package ASURV (Lavalley, Isobe, & Feigelson 1992), and we apply the following tests to each pair of parameters: the Cox proportional hazard model, the generalized Kendall rank and the Spearman rank test. The probabilities of a correlation occurring by chance in these tests are presented in Table 1 (column 4), where the probability obtained from the Cox, Kendall, and Spearman rank tests are listed in that order. The number of line measurements studied and the number of upper limits included is also shown. We considered a correlation significant only if the probability of a correlation occurring by chance in all tests was less than 1% and the fraction of upper limits was less than 1/3. For comparison we also calculate the probability of a chance correlation for data that incorporate only detections. In Table 1 we also quote the slopes and the intercept coefficients for correlations, calculated using both all data and detections only.

We find significant correlations between L_{2500} and the equivalent widths of the following emission lines: Lyα, Si IV + O IV] λ1400, C IV, Al III, Mg II. These correlations are displayed in Figure 1, with their correlation and regression results in Table 1. The slope of the Lyα Baldwin effect in our sample (β_w(Lyα) $= -0.27 \pm 0.07$) is steeper than the slope of -0.12 ± 0.05 obtained by Kinney et al. (1990), for a compilation of 114 *IUE* spectra combined with measurements from several previously published studies. Our measured slope is also steeper than that obtained by Espey & Andreadis (1999; EA99 hereafter), who analyzed the *IUE* and *HST* spectra of a heterogeneous sample of 200 AGN to obtain -0.08 ± 0.03. This may be the result of a smaller luminosity range covered by our sample (1 dex) compared to the other samples (4-5 dex), since it has been noted that the slope of the Baldwin effect flattens with increasing luminosity range (e.g. Netzer, Laor, & Gondhalekar 1992). For the C IV and Mg II Baldwin effect, our

[2] The optical iron emission appears to be predominantly FeII (Boroson & Green 1992).

luminosity range is slightly larger than that for Lyα, and we still find slopes that are slightly steeper than some previous studies. By comparison, β_w(CIV) was found to be $-0.17 \pm 0.04, -0.17 \pm 0.03$, and -0.13 ± 0.03 by Kinney et al. (1990), EA99, and Zamorani et al. (1992) respectively, while we find -0.23 ± 0.02. Slopes β_w(MgII) were found to be $+0.01 \pm 0.04$ and -0.08 ± 0.03 by EA99, and Zamorani et al. (1992) respectively, while we find -0.19 ± 0.02.

We note that sensitivity to detecting any significant correlation is affected not only by the S/N of the spectra, but also by the luminosity range spanned by each emission line in the sample. The spectral coverage and flux limits of any uniform sample will yield a maximum redshift/luminosity range for lines whose rest wavelengths are near the short wavelength end of the observed-frame spectra. Consequently, for the LBQS spectra, the luminosity range of Mg II and $\mathrm{Fe_{UV}}$ are best (2.6dex), while shorter wavelength lines like Lyα span $\sim$ 1dex, and optical lines (e.g., Hβ, [O III]) span $\sim$ 1.5dex in luminosity. Several studies cited above present larger luminosity ranges for some of the lines we investigate here. In the present work, we confine ourselves primarily to homogeneous measurements of a uniformly-selected sample. A followup paper will combine similar measurements of other samples to cover larger portions of the $L - z$ plane.

Most studies have shown little evidence for an EBEff in the SiIV+OIV] blend, although here we confirm with $\sim$400 QSOs the significant correlation noted by Laor et al. (1995) from *HST* spectroscopy of just 14 QSOs. We do not confirm the Baldwin effect found by Zheng, Kriss & Davidsen (1995) in Lyβ+O VI measurements. However, if we analyze only the detections, we do find a significant correlation (see Table 1 and Figure 2a). The slope of this correlation (-0.50 ± 0.19) is consistent within the errors with the slope found by Zheng, Kriss & Davidsen (1995; -0.30 ± 0.03). These results show that including upper limits in the analysis can help to avoid spuriously significant correlations. However, as noted by Green (1998) the Zheng et al. result is probably still valid, as the O VI emission was detected for every QSO in their sample and no upper limits have been ignored in the analysis. This may imply that we find no O VI Baldwin effect due to a smaller luminosity range covered by our sample (1 dex cf. 5 dex in Zheng et al.).

We also find a marginal Baldwin effect for Hδ and He IIλ4686, where 72% and 83% of the data respectively are non-detections. It is, however, reassuring that Wilkes et al. (1999), who study a heterogeneous sample of X-ray bright AGN, find the Hδ Baldwin effect for a sample which includes only 30% non-detections. We also find a marginal Baldwin effect for the following forbidden lines [Ne V], [O II], [Ne III] and a trend for the [O III] equivalent width to correlate with L_{2500}. We call these trends marginal because the measurements consist of 50-75% upper limits, but they are worthy of further investigation in samples of higher S/N.

We do not confirm the CIII] Baldwin effect first reported as an IBEff by Zheng, Fang & Binette (1992) for Fairall 9 and then by Green (1996) as a EBEff for a sample of 85 QSOs with *IUE* spectra. While the CIII] EBEff has $P_{Cox} < 0.01$, it does not meet our criteria for the other correlation tests. We also cannot confirm the He II λ1640 Baldwin effect found by Green (1996). Neither do we see a significant EBEff for NV, similar to Korista et al. (1998). A shallow, or even *positive correlation* with luminosity has been reported elsewhere for NV (EA99), and has been attributed to abundance effects (Hamann & Ferland 1993, HF93 hereafter). We discuss this further below in § 5 and § 6. Unfortunately, in many AGN spectra, NV is difficult to deblend from Lyα(see also discussion in HF93). The effects of blending are much less pronounced in Lyα itself, since it is by a factor of 3-4 the stronger of the two lines.

3. THE IRON BALDWIN EFFECT

Many spectra show optical and ultraviolet (UV) iron emission blends (e.g. Wills, Netzer, & Wills 1985; Boroson & Green 1992) which appear most strongly around the Hβ+[OIII] complex and the Mg IIλ2798 line. We model this emission in our spectra by independently fitting the optical template of Boroson & Green (1992), covering 4400Å$< \lambda_{rest} <$7000Å, and and the UV template of Vestergaard & Wilkes (2001), covering 1250Å$< \lambda_{rest} <$ 3100Å. For further details on the iron modeling see Paper I. We report for the first time a significant Baldwin effect for UV iron emission ($P < 10^{-4}$; 31% of 953 measurements are upper limits). We may be particularly sensitive to detecting the trend because the range of luminosity over which we can measure $\mathrm{Fe_{UV}}$ emission in the LBQS sample is larger than for any other emission line (about 3 orders of magnitude). We note that most of the upper limits occur for $z > 1.4$, which corresponds closely to log $L_{2500} \gtrsim 31$ in the LBQS (see Figure 3). To confirm our results, we excluded these objects from the sample and reran the ASURV analysis. The BEff is still highly significant ($P < 10^{-4}$; 16% of 611 measurements are upper limits). The correlation also remains strong when only the (659) detections are analyzed.

We find only a marginal Baldwin effect for optical Fe II emission ($P = 10^{-4}$ but 44% of the measurements are upper limits). The optical iron correlation is not significant in the LBQS if only detections are analyzed. Our current analysis emphasizes consistent measurements of homogeneous samples, but we may also benefit by combining with other such samples to extend the luminosity range. We therefore analyze the only other such sample currently available to us, the optical spectra of 87 QSOs - the Palomar-Green (PG) sample of Boroson & Green (1992). The luminosity range is thereby just slightly extended down to log $L_{2500} = 28.94$. We measured the strengths of Hβ, [O III], He IIλ4686, and $\mathrm{FeII_{opt}}$ emission using the automated technique described in Paper I. The combined PG and LBQS sample detects a significant Baldwin effect for $\mathrm{FeII_{opt}}$ (where 33% of data in the combined sample are comprised of upper limits). No other new significant trends are detected in the PG+LBQS sample according to our criteria.[3]

4. EVOLUTION OF IRON EMISSION STRENGTH

[3]The He IIλ4686 EBEff is significant, but the upper limits for He II decline from 83% in the LBQS to 58% in the combined sample, still above our threshold of 1/3.

As expected in a flux-limited sample such as the LBQS, luminosity and redshift are strongly correlated, and the available range of L_{2500} decreases with redshift. A plot of log L_{2500} vs. log-redshift is shown in Figure 3. In the LBQS, L_{2500} spans a factor of ~ 50 for $z < 0.5$, 20 up until $z \sim 2$, and ~ 8 for $z > 2$. Does iron emission strength depend more on luminosity, or redshift? This question has not been discussed much in treatments of the EBEff in general (though see Baldwin, Wampler, & Gaskell 1989). This is surprising, since the finding of a stronger redshift correlation would carry the important implication that evolution is directly detectable in quasar spectra. Here we take advantage of our large sample and consistent measurements to test for the primary relationship. Astronomical measurements often correlate strongly with several variables, and multivariate statistical analyses have been performed in a number of studies in the literature. Examples include Green (1996), Eskridge, Fabbiano, & Kim (1995), Wilkes et al. (1994), and Djorgovski et al. (1993). Partial Spearman Rank Analysis (hereafter PSRA; Kendall & Stuart 1976) allows for correlation analysis in the general multivariate case, using a matrix of bivariate Spearman rank statistics as input. PSRA tests for correlations between subsamples of the matrix parameters while holding constant all other variables in the matrix. We use the ASURV bivariate Spearman Ranks as input to multivariate PSRA, and find that since the partial correlation coefficients with redshift are of larger magnitude[4] *iron equivalent width in the UV is primarily anticorrelated with redshift, not with luminosity.* $W_\lambda(\mathrm{FeII_{UV}})$ anticorrelates most strongly with redshift ($P_{PSR} < 0.005$, and a PSR of $\rho = -0.123$, while its correlation with L_{2500} has $P_{PSR} = 0.177$ and $\rho = -0.033$). To check if this result is plausibly related to the magnitude limit of the LBQS ($B_J = 18.85$), we also tested a brighter ($B_J < 18.6$) subsample of the LBQS, and found a similar result (see Table 2). We discuss this subsample further in § 5 below.

Our finding of iron evolution is supported by the recent comparison by Kuhn et al. (2001) of two QSO samples *matched in evolved luminosity.* [5] They also found evidence for a decrease with redshift of the strength of the 2200-3000Å bump.

While iron is produced in all supernovae (SN), the dominant producer appears to be SN Ia (HF93; Wheeler et al. 1989). Since SN Ia progenitors have a lifetime of ∼1 Gyr, large increases in iron abundance could be delayed for at least that amount of time after the first epoch of star formation. For $q_0 = 0.5$, the age of the Universe is $1(h^{-1})$Gyr at $z \sim 3$. Thus as proposed by HF93, detection of this abundance shift might enable cosmological tests. In contrast to iron, magnesium production should be dominated by type II, Ia, and Ib supernova, so that changes in the Fe/MgII ratio should be most evident around the epoch when SN Ia become prevalent. Thompson, Hill, & Elston (1999) designed a test for this effect comparing three composite spectra: two averages of 6 QSOs each with mean redshifts of $\overline{z} \sim 3.4$ and $\overline{z} \sim 4.5$, and an LBQS composite with $\overline{z} \sim 0.8$. They found that the Fe/MgII was constant within their measurement errors. However, this ratio is certainly complicated by the strong MgII EBEff that we and others detect. When Thompson et al. attempted an independent iron measurement, they found $W_\lambda(\mathrm{FeII_{UV}})$ to be "marginally larger" in the highest redshift composite. Unfortunately, the detailed structure of composite spectra depends on how and where their constituent spectra are normalized before adding (Brotherton et al. 2001), and this is especially crucial when measuring blended iron emission around the strong, broad MgII line.

5. EVOLUTION OF EMISSION LINE STRENGTH

Given the intriguing results showing that evolution of iron emission strength is a primary correlation (with luminosity secondary) we have pursued similar partial correlation analyses for all lines in our sample. Partial correlation results are presented in Table 2 for all lines showing a significant correlation with either luminosity or redshift. For the full LBQS sample, the influence of evolution on emission line strength appears to dominate for all lines, since the probability P of a null correlation is significantly smaller when redshift rather than luminosity is allowed to vary. The equivalent widths of Lyα, C IV, Al III, Si IV, C III], Mg II, $\mathrm{Fe_{UV}}$, and Hβ all decrease with increasing redshift, with a stronger dependence on redshift than on luminosity. The evolution regressions for all significant W_λ-redshift correlations in the full sample are listed in Table 3, and drawn over the data (as dashed lines) in Figure 4 for correlations that show significant correlations separately with both luminosity and redshift. Identical ranges in logW_λ are used as in Figure 1 to allow a direct comparison. We perform a simple analysis that we find to be an intuitive reflection of the visual impression that evolution plots have less dispersion than EBEff plots. We subtract the best-fit regression for those correlations also with a significant EBEff in Table 1, and derive the residual RMS dispersion.[6] We find smaller RMS dispersions generally for the correlation we designate as primary from the PSRA results in Table 2. For this exercise, we only compared correlations that were significant both for the EBEff and for evolution. Neither C III] nor Hβ are included, since we detected no significant trend with luminosity. Their correlations with redshift are significant, and are plotted in Figure 5.

The distribution of W_λ upper limits is typically weighted towards high luminosities and high redshifts, which if it is an observational effect could bias a correlation or a regression when the fraction of limits is large. To test the effect of this potential bias, we also ran partial correlation analyses on W_λ as a function of log L_{2500} and log z for the subset of data that excludes line upper limits. The correlation results for this sample are also shown in Table 2. The primary correlation appears to still be redshift for Lyα, Si IV, and C IV. The $\mathrm{Fe_{UV}}$ results for detections only are ambiguous, since the correlation coefficients (ρ) for log z and log L_{2500} are identical. In any case, since exposure times for the LBQS spectra achieved

[4]Or correspondingly, the probability P of a null correlation, is significantly smaller when redshift rather than luminosity is allowed to vary.

[5]Both their high and low redshift samples span the range $1 < L/L_*(z) < 7$, where $L_*(z) = L_*(1+z)^k$, the optical luminosity function parameterization of pure luminosity evolution from Boyle, Shanks, & Peterson (1988).

[6]Since the RMS is difficult to define when including upper limits, we examine detections only, and use the relevant regressions listed in Table 1 and Table 3.

very similar median S/N ratios across the range of B_J mag, the appearance of weaker lines at higher redshift is most likely due to an intrinsic effect.

Similarly, since our results are plausibly biased by the magnitude limit of the LBQS ($B_J = 18.85$), we also tested a brighter ($B_J < 18.6$) subsample of the LBQS. Given that the magnitude range of this bright subsample is from 16 to 18.6, it only covers about an order of magnitude in blue flux, and therefore samples a different part of the luminosity function at each redshift. However, the effects of Malmquist biases and pileup at the sample flux limit are relieved, since every true $B_J = 18.6$ source was easily detected. The mag errors are also lower than at the survey limit, so that fewer faint quasars land in the brighter subsample due only to photometric errors, and there is less random error in the derived log L_{2500} values. For the $B_J < 18.6$ subsample, all correlations which show an EBEff have their primary correlation with redshift (Table 2).[7]

6. TRENDS WITH IONIZATION POTENTIAL

Zheng, Fang & Binette (1992) analyzed the *IUE* spectra of the highly variable AGN Fairall 9 and found that the slope of the intrinsic Baldwin effect becomes steeper for lines with higher ionization potential. Zheng, Kriss & Davidsen (1995) found a similar trend in a small sample of 32 QSOs and Seyfert 1 galaxies (observed by *IUE*, *HST*, and HUT). The EBEff showed the steepest slope for the O VI line (with the highest potential), followed by the slopes of C IV and Lyα. This finding was later confirmed by EA99, who studied a larger number of UV and optical line slopes for a heterogeneous sample of ∼200 AGN and found a trend ($P < 5\%$) that lines with increasing ionization potential show a steeper Baldwin effect slope (see their Figure 4).

We present the dependence of the EBEff slope on ionization potential in our LBQS sample in Figure 6. Open circles represent the slopes calculated for all LBQS data (from Table 1) with our linear fit shown by a dashed line. The slopes we calculate for detections only are represented by filled squares, with the best-fit slope shown with a solid line. Our best-fit linear "slope-of-slopes" (SOS) regressions for detections only (-0.0026 ± 0.0007) and all data (0.0003 ± 0.0237) are consistent within the errors with that found by EA99 (-0.0015 ± 0.0005). However the correlation between slope and the ionization potential is not significant in our sample, with or without emission line upper limits included ($P = 90\%$ and $P = 30\%$ respectively). The lack of a correlation is in part the result of relatively steep EBEff slopes we measure for the low ionization potential lines Lyα and $\mathrm{Fe_{UV}}$. The steep Lyα slope we measure is probably caused by the rather small luminosity range covered for this wavelength in the LBQS sample (see Netzer et al. 1992). No $\mathrm{Fe_{UV}}$ slope was included in EA99. As described in § 3, an $\mathrm{FeII_{opt}}$ EBEff is excluded as insignificant by our adopted criteria, unless the PG sample is included. Inclusion of the PG sample shifts the $\mathrm{FeII_{opt}}$ EBEff slope from −0.45 (see Table 1) to −0.28, but the resulting SOS relation remains insignificant ($P \sim 90\%$).

It would be intriguing if ionization potential yielded a significant correlation, since the production of many emission lines may be sensitive to continuum photons both softer and harder than the ionization potential of the species in question, because such photons may ionize from excited states and also heat the gas via free-free and H^- absorption. For example, in most photoionization models (e.g., Krolik & Kallman 1988), UV Fe originates at low optical depths in BLR clouds where EUV and soft X-ray photons contribute to heating. FeII emission in the optical is principally due to higher energy photons (above ∼ 800eV). Ionization from excited states and heating via free-free and H^- absorption also help determine the principal ionizing/heating continuum (Krolik & Kallman 1988) of an emission line. Perhaps more representative energies than the ionization potential should be used in the SOS plot, or lines that respond most significantly to heating could be excluded. The former involves many changes and considerable uncertainty in the chosen energies, while the latter does little to forge a significant correlation.

We do not include a NV EBEff slope in the above discussion, because it was not significant in the LBQS. The N V line was excluded from the slope of slopes figure of EA99 as well, because it did not fit the overall relation. It was claimed that the aberrant slope of NV is due to abundance changes with redshift (Korista et al. 1998; Hamann & Ferland 1999), which we discuss briefly below.

7. DISCUSSION

The observed decrease of $W_\lambda(\mathrm{Fe_{UV}})$ with redshift, if confirmed, corresponds to an increase of $W_\lambda(\mathrm{FeII_{UV}})$ with cosmic time that could be attributable to a number of evolutionary effects including: (1) a increase in iron abundance (2) an increase in the covering factor of iron-emitting clouds or (3) a shift in continuum SEDs or (4) of gas conditions (i.e. density, temperature, or ionization) in the emitting clouds. If the significant evolutionary trends that we detect in this and other measured emission lines are the result of abundance changes, they proceed with the arrow of cosmic time in the expected sense; abundances increase with time as more stars cycle metals into the interstellar medium, thereby enhancing the abundances of clouds in the nuclear environment of quasars. However, most previous claims of detected trends in the metallicity of QSO emission line clouds appear to go in the opposite sense (Hamann & Ferland 1999; Vernet et al. 2001). Those less intuitive trends, if true, might be explained if QSOs at higher redshifts are more luminous (generally true in flux-limited samples) and also more massive, analogous to the mass-metallicity trend observed in nearby elliptical galaxies (e.g., Köppen & Arimoto 1990). Another explanation might be that the most effective metallicity enhancements occurred at early cosmological epochs, but high redshift QSOs are short-lived and unrelated to low-redshift counterparts (HF93). Are abundances larger in the BLR at early or late epochs? A determination of the correct answer is important, since it provides a potential measure of the epoch and lifetime of nuclear activity in galaxies.

Line ratios may be more robust indicators of metallicity then the equivalent width trends we emphasize within the scope of this paper. The measurements we provide in Paper I provide the basis for our pursuit of further line

[7]However, W_λ(C III]) correlates significantly with neither luminosity ($P_S = 0.081$) or redshift ($P_S = 0.045$) in the $B_J < 18.6$ subsample.

ratio studies. Nitrogen intensity should be particularly sensitive to metallicity since as a secondary element, it goes up roughly as the square of the metallicity (Z) in scenarios of rapid star formation. Expected line ratios for solar metallicity gas are ~ 0.1 for NV/CIV and ~ 1 for NV/HeII (Hamann & Ferland 1999). Ferland et al. (1996) found some robustly large NV/HeII ratios in luminous QSOs, requiring $Z \gtrsim 5 Z_{\odot}$. Dietrich & Wilhelm-Erkens (2000) similarly derive $Z \gtrsim 8 Z_{\odot}$ for a sample of 16 QSOs ($2.4 < z < 3.8$).The correlation of NV/CIV with NV/HeII (Hamann & Ferland 1999; Vernet et al. 2001) seems likely to be an abundance effect (Villar-Martin et al. 1999).

There are caveats, however. NV and CIV are produced in different regions, and their ratio is only linear in Z. Because of the substantial cooling afforded by CIV, an increase in abundance could be accompanied by a decrease in temperature, which in turn reduces the response of line strength to abundance; weak lines respond better. While NV and HeII lines arise in regions of similar ionization, both are notoriously difficult to measure in the majority of QSOs because they are broad and often strongly blended with nearby lines. Perhaps more importantly, we reiterate that the measurements of NV that dominate discussions of abundance are generally very difficult due to blending with the much stronger Lyα line. The proximity of NV to Lyα also means that outflowing clouds (e.g., as seen in BALs) may boost NV emission because of resonant scattering of Lyα in the restframe of the cloud (Krolik & Voit 1998). Studies of broad absorption lines in quasars may help (Korista et al. 1996). These also suggest high BAL cloud abundances of up to $10 Z_{\odot}$, where rapid star formation models yield better abundance fits than do scaled solar metallicities. The interpretation of BAL measurements is in flux, however, since the BAL profiles seem to be determined more strongly by partial covering than by optical depth (Arav et al. 1999).

Is the detected trend of iron an abundance effect? Within photoionization models, the effect of abundance on iron line strength is very weak due to the thermostatic effect of Fe II. Indeed, photoionization models have severe trouble accounting for the observed strength of iron emission (Collin & Joly 2000), requiring the iron emitting region to be heated by an additional, non-radiative mechanism. Wind models look promising because outflows (1) could produce the shocks and consequent non-radiative heating; (2) may shield the narrow line region (NLR) or even replace it with a denser medium. Furthermore, there are analogies in stellar winds that are observed to produce both a sort of intrinsic Baldwin Effect (Morris et al. 1993) and strong iron emission (e.g., Hillier & Miller 1998). So the underlying cause of the observed line evolution might be evolution in outflows (e.g., Murray & Chiang 1998), which may in turn be caused by evolution of black hole mass and accretion rate (e.g., Wandel 1999b). Studies of broad line width as a function of look-back time can help address this question.

Because evolution predominates in our sample even for W_{λ}(Lyα), the trends we detect are indeed more likely to correspond to evolution in cloud conditions rather than in abundance (although the two are linked by thermostatic effects). Each QSO observable is an axis in a multidimensional space where that can be transformed using principal component analysis (PCA) into a new basis space whose first eigenvector represents most of the diversity in QSO spectra, and is a linear combination of the original axes (observables) . About 50% of QSO optical/UV spectral diversity can thus be projected along a principal eigenvector of spectral properties dubbed Eigenvector 1 (or PC1; Boroson & Green 1992; Wills et al. 1999, and references therein). Linking such measurables as FWHM(Hβ), FeII/Hβ, SiIII]/CIII], W_{λ}(C IV), W_{λ}([O III]), and X-ray spectral slope α_x, PC1 has been hypothesized to reflect accretion rate L/L_{Edd} and/or the presence of outflowing winds. Narrow line Seyfert 1s (NLS1s) and low-ionization broad absorption line (loBAL) quasars share several properties that appear to lie at one extreme of PC1. Among them are weak narrow line but strong iron emission, narrow FWHM(Hβ), and perhaps evidence of outflows (Brandt 2000; Mathur 2000a) and steep (soft) intrinsic α_x(Mathur et al. 2001). One possibile explanation of larger $\mathrm{Fe_{UV}}$ equivalent widths in the present epoch is that outflows are now more common. Debate has begun on whether the accretion rate is large in the early or late phases of evolution (Mathur 2000b; Wandel 1999c; Wilman & Fabian 1999). If outflows indeed dominate $\mathrm{Fe_{UV}}$ line strength, then our work here suggests the latter.

We do not propose that redshift/emission line correlations reported here completely explain the ensemble Baldwin effect. Significant EBEffs have been seen in samples spanning very small redshift ranges (e.g., Netzer et al. 1992; the $0.08 < z < 0.4$ sample of Wills et al. 1999). Furthermore, as described above (§ 1, even individual AGN observed at multiple epochs (a 'sample' with zero redshift range) exhibit an intrinsic W_{λ}-luminosity anticorrelation (Kinney et al. 1990; Pogge & Peterson 1992). Rather, here we find new evidence that evolution may also play a role in the EBEff, and could be the primary correlation for several important lines. The simplest use of the EBEff to constrain cosmological parameters like q_0 is similar to main sequence fitting of star clusters, in that it depends on the assumption of no (or at least predictable) evolution (Baldwin 1999). Since evolution of the quasar luminosity function is well-accepted, it is reasonable to also expect evolution in other observables like emission line strength. Rather than using quasars to measure q_0, it will likely turn out instead that other methods of measuring cosmological parameters (see § 1) will provide a cosmology sufficiently precise that we can then make more rapid progress understanding quasar evolution, particularly at high redshifts.

The current study suffers from several problems. First, the typical S/N of the LBQS spectra are too low, with a median of ~ 5 averaged over the entire observed spectrum. Second, the sample has a single relatively bright flux limit, so that L and z are strongly correlated. The ideal study would measure two large quasar samples at very different redshifts, each spanning a wide but similar range of L, selected without regard to emission line strength, and with high S/N spectra available. As long as we're making a wish list, multi-epoch spectroscopy for such samples would also be valuable, for reasons outlined in the introduction. Variability anticorrelates with luminosity in AGN (Webb & Malkan 2000; Giveon et al. 1999), and there is no evi-

dence that variability correlates in any way with redshift (Helfand 2001; Hawkins 2000).

Extension of this study of the LBQS sample to lower redshifts and luminosities using consistent measurement techniques is clearly of interest to fill in the luminosity-redshift plane of Figure 3 and alleviate the degeneracy imposed by the strongest correlation in the current sample. We are pursuing such a study by measuring a large but heterogeneous sample of *HST* FOS spectra (Kuraszkiewicz et al. 2001), and expect that the results should prove convincing since the spectral coverage includes most of the same UV emission lines analyzed here. The emission line properties of the optically-selected quasars from the Sloan Digital Sky Survey (SDSS - Richards et al. 2001; York et al. 2000) could provide a large sample of great diversity. On the other hand, optical samples may highlight only the brief juncture in QSO evolution when luminosities are still large, but enshrouding material has been blown away (Wilman & Fabian 1999). Spectroscopy of upcoming X-ray selected samples from Chandra (ChaMP; Green et al. 1999; Wilkes et al. 2001), similarly analyzed, holds great promise to unravel the complexities of quasars' intrinsic physics from their evolution over the span of the observable Universe.

The authors gratefully acknowledge support provided by NASA through grant NAG5-6410 (LTSA). We are grateful to Craig Foltz for providing the LBQS spectra, to Todd Boroson for providing the spectra of the PG QSOs, and to Jack Baldwin for providing his comments on a draft of this manuscript.

REFERENCES

Arav, N, Korista, K.T., de Kool, M., Junkkarinen, V. T., & Begelman, M. C. 1999, ApJ, 516, 27
Baldwin, J.A. 1977, ApJ, 214, 679
Baldwin, J.A., Wampler, E. J., & Gaskell, C. M. 1989, ApJ, 338, 630
Baldwin, J. A. 1999, in *Proceedings of Quasars as Standard Candles for Cosmology*, eds. J. Baldwin & G. J. Ferland (San Francisco: Astronomical Society of the Pacific) v162, 475
Boroson, T.A., & Green, R.F. 1992, ApJS, 80, 109 (BG92)
Boyle, B. J., Shanks, T., & Peterson, B. A. 1988, MNRAS, 243, 231
Brandt, W. N. 2000, NewAR, 44, 461
Brotherton, M. S., Tran, H. D., Becker, R. H., Gregg, M. D., Laurent-Muehleisen, S. A., & White, R. L. 2001, ApJ, in press.
Collin, S. & Joly, M. 2000, NewAR, 44, 531
Dietrich, M.& Wilhelm-Erkens, U. 2000, A&A, 354, 17
Djorgovski, S., Piotto, G., Capaccioli, M. 1993, AJ, 105, 2148
Eskridge, P. B., Fabbiano, G., & Kim, D.-W. 1995, ApJS, 97, 141
Espey, B. & Andreadis, S. 1999, in *Proceedings of Quasars as Standard Candles for Cosmology*, eds. J. Baldwin & G. J. Ferland (San Francisco: Astronomical Society of the Pacific) v162, p351 (EA99)
Fan, X., White, R. L., Davis, M., et al. 2000, AJ, 120, 1167
Ferland, G. J. et al. 1996, ApJ, 461, 683
Forster, K, Green, P. J., Aldcroft, T., Vestergaard, M., & Foltz, C. B. 2001, ApJS, 134, in press (Paper I)
Garnavich, P. M., Kirshner, R. P., Challis, et al. 1998, ApJ, 493, 53
Giveon, U., Maoz, D., Kaspi, S., Netzer, H., & Smith, Paul S. 1999, MNRAS, 306, 637
Green, P. J., et al. 1995, ApJ, 450, 51
Green, P. J. 1996, ApJ, 467, 61
Green, P. J. 1998, ApJ, 498, 170
Green, P. J. 1999, in *Proceedings of Quasars as Standard Candles for Cosmology*, eds. J. Baldwin & G. J. Ferland (San Francisco: Astronomical Society of the Pacific) v162, p351
Hamann, F. & Ferland, G.J. 1993, ApJ, 418, 11 (HF93)
Hamann, F. & Ferland, G. J. 1999, ARAA, 37, 487
Hawkins, M. R. S. 2000, A&AS, 143, 465
Helfand, D. J., Stone, R.P.S., Willman, B., White, R. L., Becker, R. H., Price, T., Gregg, M. D., & McMahon, R.G. 2001, AJ, in press
Hillier, D. J. & Miller, D. L. 1998, ApJ, 496, 407
Iwasawa, K. & Taniguchi, Y. 1993 , ApJ, 413, 15
Kendall, M., & Stuart, A. 1976, The Advanced Theory of Statistics, Vol. II (New York: Macmillan).
Kinney, A. L., Rivolo, A.R., & Koratkar, A.P. 1990, ApJ, 357, 338
Köppen, J. & Arimoto, N. 1990, A&A, 240, 22
Korista, K. T., Hamann, F. W., Ferguson, J. W., & Ferland, G. J. 1996, ApJ, 461, 641
Korista K. T., Baldwin J. A., & Ferland, G. J. 1998, ApJ, 507, 24
Krolik, J. H., & Kallman, T. R. 1988, ApJ, 324, 714
Krolik J. & Voit G. M. 1998. Ap. J. 497, L5
Kuraszkiewicz, J., Green P. J., Forster, K., Evans, I., & Koratkar, A. 2001, in preparation
Krolik, J. H., & Kallman, T. R. 1988, ApJ, 324, 714
Kuhn, O., Elvis, M., Bechtold, J., & Elston, R. 2001, ApJS, submitted
Lavalley, M., Isobe, T., & Feigelson, E. D. 1992, ADASS, 1, 245
Laor, A. et al. 1995, ApJS, 99, 1
Mathur, S. 2000a, NewAR, 44, 7-9
Mathur, S. 2000b, MNRAS, 314, 17
Mathur, S., Matt, G., Green, P. J., Elvis, M., & Singh, K. P. et al. 2001, in preparation.
Melchiorri, A., Ade, P. A. R., de Bernardis, P., et al. 2000, ApJL, 536, 63
Morris, P., Conti, P. S., Lamers, H. J. G. L. M., Koenigsberger, G. 1993, ApJL, 414, 25
Murray, N. & Chiang, J 1998, ApJ, 494, 125
Netzer, H., Laor, A., & Gondhalekar, P.M. 1992, MNRAS 254, 15
Osmer, P.S., Porter, A.C., & Green, R.F. 1994, ApJ, 436, 678
Park, C., Colley, W. N., Gott, J., R., Ratra, B., Spergel, D. N., & Sugiyama, N. 1998, ApJ, 506, 473
Perlmutter, S. et al. 1999, ApJ, 517, 565
Pogge, R.W., & Peterson, B. 1992, AJ, 103, 1084
Reeves, J. N. et al. 2001, A&A 365, L116
Richards, G. T. et al. 2001, AJ, in press
Sergeev, S. G., Pronik, V. I., Sergeeva, E. A., Malkov, Y. F. 1999, AJ, 118, 2658
Shields, J. C., Ferland, G. J., & Peterson. B. M. 1995, ApJ, 441, 507
Thompson, K. L., Hill, G. J., Elston, R. 1999, ApJ, 515, 487
Tytler, D., & Fan X.-M. 1992, ApJS, 79, 1
Vestergaard, M., & Wilkes, B.J. 2000, ApJ, submitted.
Vernet, J., Fosbury, R. A. E., Villar-Martin, M., Cohen, M. H., Cimatti, A., di Serego alighieri, S., & Goodrich, R. W. 2001, A&A, 366, 7
Villar-Martin, M., Vernet, J., Fosbury, R. A. E., Binette, L., Tadhunter, C. N., & Rocca-Volmerange, B. 1999, A&A, 351, 47
Webb, W. & Malkan, M. 2000, ApJ, 540, 652
Wheeler J. C., Sneden C., & Truran J. W. 1989, ARAA, 27, 279
Wandel, A. 1999a, ApJ, 527, 649
Wandel, A. 1999b, ApJ, 527, 657
Wandel, A. 1999c, ApJL, 519, 39
Wilkes, B. J., Kuraszkiewicz, J., Green, P. J., Mathur, S., & J.C. McDowell 1999, ApJ, 513, 76
Wilkes, B. J. et al. 2001, in *New Era of Wide Field Astronomy*, eds. Clowes, R.G., Adamson, A.J., & Bromage, G.E. (San Francisco: Astronomical Society of the Pacific), in press
Wilkes, B. J., Tananbaum, H., Worrall, D. M., Avni, Y., Oey, M. S., & Flanagan, J. 1994, ApJS, 92, 53
Wills, B.J., Netzer, H., & Wills, D. 1985, ApJ, 288, 94
Wills, B.J., Laor, A., Brotherton, M. S., Wills, D., Wilkes, B. J., Ferland, G. J., & Shanf, Z. 1999, ApJ, 515, L53
Wilman, R. J. & Fabian, A. C. 1999, ApJ, 522, 157
Wu, C.-C., Boggess, A., & Gull, T. R 1983, ApJ, 266, 28
York, D., et al. 2000, AJ, 120, 1579
Zamorani, G., Marano, B., Mignoli, M., Zitelli, V., & Boyle, B. J. 1992, MNRAS, 256, 238
Zheng, W., Fang, L.-Z., & Binette, L. 1992, ApJ, 392, 74
Zheng, W., Kriss, G.A., & Davidsen, A.F. 1995, ApJ, 440, 606

TABLE 1
BALDWIN EFFECT REGRESSIONS FOR THE LBQS

Emission line			All Data (including upper limits)			Detections only			
Line Name	N_{Tot}	N_{Limits}	C/K/S [a]	Slope	Intercept	N	C/K/S [a]	Slope	Intercept
Fe UV	953	294	**0.00/0.00/0.00**	-0.617 ±0.047	20.2 ± 1.4	659	**0.00/0.00/0.00**	-0.105 ± 0.016	4.8 ± 0.5
Fe II opt	248	110	**0.00/0.00/0.00**	-0.447 ± 0.108	14.5 ± 3.2	138	0.47/0.35/0.36	-0.007 ± 0.034	1.7 ± 1.0
Lyβ λ1025.7 + O VI λ1035	130	27	0.98/0.19/0.22	0.112 ± 0.221	-2.9 ± 7.0	103	**0.00/0.00/0.00**	-0.500 ± 0.187	16.7 ± 5.9
Lyα λ1215.7	259	0	**0.00/0.00/0.00**	-0.272 ± 0.067	10.3 ± 2.1	259	**0.00/0.00/0.00**	-0.272 ± 0.067	10.3 ± 2.1
N V λ1241.5	259	8	0.72/0.35/0.41	-0.037 ± 0.060	2.3 ± 1.9	251	0.01/0.08/0.09	-0.128 ± 0.068	5.2 ± 2.2
O I λ1305	259	120	0.10/0.15/0.04	-0.266 ± 0.121	8.5 ± 3.8	139	0.05/0.02/0.03	-0.307 ± 0.114	10.1 ± 3.6
Si IV + O IV] λ1400	414	19	**0.00/0.00/0.00**	-0.300 ± 0.080	10.3 ± 2.4	395	**0.00/0.00/0.00**	-0.308 ± 0.050	10.7 ± 1.6
C IV λ1549	487	1	**0.00/0.00/0.00**	-0.227± 0.025	8.7 ± 0.8	486	**0.00/0.00/0.00**	-0.231 ± 0.044	8.8 ± 1.4
He II λ1640	487	68	0.00/0.23/0.20	-0.166 ± 0.097	6.2 ± 3.0	419	0.59/0.38/0.37	0.058 ± 0.077	-0.7 ± 2.4
Al III λ1859	667	181	**0.00/0.00/0.00**	-0.229 ± 0.065	7.8 ± 2.0	486	0.07/0.09/0.10	-0.064 ± 0.054	2.8 ± 1.7
C III] λ1909	667	26	0.00/0.07/0.06	-0.120 ± 0.037	5.1 ± 1.1	641	0.55/0.56/0.57	-0.034 ± 0.032	2.4 ± 1.0
Mg II λ2800	677	42	**0.00/0.00/0.00**	-0.187 ± 0.017	7.3 ± 0.5	635	**0.00/0.00/0.00**	-0.126 ± 0.023	5.4 ± 0.7
[Ne V] λ3426	488	365	**0.00/0.00/0.00**	-0.288 ± 0.054	8.9 ± 1.6	123	0.04/0.34/0.33	0.079 ± 0.079	-1.7 ± 2.3
[O II] λ3728	393	272	**0.00/0.00/0.00**	-0.337 ± 0.036	10.4 ± 1.1	121	0.32/0.20/0.24	0.059 ± 0.064	-1.0 ± 1.9
[Ne III] λ3869	363	259	**0.00/0.00/0.00**	-0.464 ± 0.069	14.3 ± 2.1	104	0.09/0.06/0.06	0.126 ± 0.061	-3.0 ± 1.8
Hδ λ4101.7	309	222	**0.00/0.00/0.00**	-0.392 ± 0.085	12.0 ± 2.6	87	0.03/0.14/0.14	-0.060 ± 0.116	2.9 ± 3.4
Hγ λ4340.5 + [O III] λ4363	251	87	0.07/0.08/0.05	-0.146 ± 0.070	5.5 ± 2.1	164	0.46/0.57/0.57	-0.029 ± 0.047	2.0 ± 1.4
He II λ4686.5	186	154	**0.00/0.00/0.00**	-0.470 ± 0.091	14.5 ± 2.7	32	0.11/0.49/0.43	0.091 ± 0.217	-1.6 ± 6.4
Hβ λ4861.3	146	16	0.07/0.08/0.09	-0.214 ± 0.083	8.1 ± 2.5	130	0.92/0.20/0.25	-0.071 ± 0.074	3.9 ± 2.2
[O III] λ4959	146	71	0.02/0.18/0.05	-0.246 ± 0.098	8.1 ± 2.9	75	0.40/0.25/0.26	0.105 ± 0.129	-2.1 ± 3.8
[O III] λ5007	146	52	0.01/0.03/0.01	-0.300 ± 0.138	10.1 ± 4.1	94	0.73/0.70/0.76	0.087 ± 0.078	-1.3 ± 2.3

[a]Correlation probabilities from ASURV for (C) Cox proportional Hazard model, (K) generalized Kendall's tau, and (S) Spearman's rho.

NOTE.—Schmitt 2-D Kaplan-Meier regression fits and errors from ASURV. The Baldwin effect examined here is log $L_{2500} \propto$ log W_λ (line). Emission line names shown in boldface meet our most stringent significance criteria: $P < 1\%$ in all 3 correlation tests using all data, and an upper limit fraction $< 33\%$. Correlation probabilities in boldface meet the former criterion for the data tested, regardless of limit fraction.

TABLE 2
PARTIAL CORRELATIONS

Line	All data (including upper limits) logW_λ vs. log L_{2500} P	ρ	logW_λ vs. log z P	ρ	Detections only logW_λ vs. log L_{2500} P	ρ	logW_λ vs. log z P	ρ
			LBQS Sample					
Fe UV	0.177	-0.033	<**0.005**	-0.123	0.175	-0.983	0.175	-0.983
Lyβ+O VI	...	...	...	...	**0.258**	-0.065	0.358	-0.037
Lyα	<0.005	0.210	<**0.005**	-0.301	<0.005	0.207	<**0.005**	-0.298
Si IV + OIV]	<0.005	0.280	<**0.005**	-0.382	<0.005	0.300	<**0.005**	-0.409
C IV	0.250	-0.031	**0.158**	-0.048	0.245	-0.032	**0.153**	-0.049
Al III	<0.005	0.142	<**0.005**	-0.207	...	...	...	...
C III]	0.066	0.060	**0.011**	-0.091	...	...	...	...
Mg II	0.154	-0.045	**0.075**	-0.063	**0.011**	-0.092	0.305	0.021
Hβ	<0.005	0.313	<**0.005**	-0.378	<0.005	0.286	<**0.005**	-0.338
			LBQS $B_J < 18.6$ Subsample					
Fe UV	0.177	-0.033	<**0.005**	-0.123	0.244	-0.030	**0.208**	-0.037
Lyα	<0.005	0.379	<**0.005**	-0.446	<0.005	0.161	<**0.005**	-0.258
Si IV + OIV]	...	...	...	...	<0.005	0.164	<**0.005**	-0.272
C IV	0.239	0.037	**0.024**	-0.103	0.244	0.036	**0.023**	-0.104
Al III	<0.005	0.151	<**0.005**	-0.204	...	...	...	...
Mg II	>0.400	0.000	**0.012**	-0.098	**0.181**	-0.041	0.257	-0.028
Hβ	<0.005	0.520	<**0.005**	-0.565	<0.005	0.535	<**0.005**	-0.568

NOTE.—P is the partial Spearman rank probability and ρ is the partial correlation coefficient of that W_λ correlation occurring by chance, given that W_λ may depend on both log L_{2500} and log z, and holding each of these variables constant in turn. Bold fonts denote the primary correlation for each line. No values are listed for correlations that are not significant (i.e., have $P < 0.01$ and $< 33\%$ upper limits) in either independent variable singly.

TABLE 3

EVOLUTION REGRESSIONS FOR LBQS EMISSION LINES

Emission line			All Data (including upper limits)				Detections only		
NAME	TOT	UPP	C/K/S [a]	Slope	Intercept	NUM	C/K/S	Slope	Intercept
				Full LBQS					
Fe UV	953	294	**0.00/0.00/0.00**	-1.312±0.101	1.13±0.03	659	**0.00/0.00/0.00**	-0.190±0.038	1.52±0.01
Lyα	259	0	**0.00/0.00/0.00**	-1.199±0.227	2.19±0.08	259	**0.00/0.00/0.00**	-1.216±0.226	2.20±0.08
Si IV + O IV]	414	19	**0.00/0.00/0.00**	-1.045±0.153	1.29±0.05	395	**0.00/0.00/0.00**	-1.163±0.149	1.35±0.05
C IV	487	1	**0.00/0.00/0.00**	-0.480±0.063	1.69±0.02	486	**0.00/0.00/0.00**	-0.481±0.107	1.69±0.03
Al III	667	181	**0.00/0.00/0.00**	-0.788±0.185	0.75±0.03	486	0.06/0.03/0.04	-0.202±0.092	0.87±0.02
C III]	667	26	**0.00/0.01/0.01**	-0.255±0.078	1.41±0.01	641	0.60/0.24/0.26	-0.045±0.069	1.40±0.01
Mg II	677	42	**0.00/0.00/0.00**	-0.390±0.044	1.49±0.02	635	**0.00/0.00/0.00**	-0.230±0.055	1.54±0.01
Hβ	146	16	**0.00/0.00/0.00**	-0.834±0.228	1.26±0.13	130	0.05/0.02/0.02	-0.561±0.171	1.45±0.09
				LBQS bright					
Fe UV	777	233	**0.00/0.00/0.00**	-1.283±0.079	1.12±0.02	544	**0.00/0.00/0.00**	-0.178±0.036	1.52±0.01
Lyα	198	0	**0.00/0.00/0.00**	-1.071±0.270	2.14±0.09	198	**0.00/0.00/0.00**	-1.071±0.270	2.14±0.09
Si IV	323	14	**0.00/0.00/0.00**	-0.902±0.178	1.26±0.05	309	**0.00/0.00/0.00**	-1.102±0.122	1.34±0.03
CIV	383	1	**0.00/0.00/0.00**	-0.492±0.136	1.68±0.04	382	**0.00/0.00/0.00**	-0.488±0.103	1.68±0.03
Al III	529	134	**0.00/0.00/0.00**	-0.689±0.140	0.76±0.03	395	0.05/0.05/0.06	-0.206±0.091	0.86±0.02
Mg II	562	33	**0.00/0.00/0.00**	-0.396±0.051	1.48±0.01	529	**0.00/0.00/0.00**	-0.248±0.058	1.53±0.01
Hβ	124	12	**0.00/0.00/0.00**	-0.976±0.327	1.17±0.19	112	0.05/0.02/0.01	-0.571±0.238	1.44±0.13

[a]Correlation probabilities from ASURV for (C) Cox proportional Hazard model, (K) generalized Kendall's tau, and (S) Spearman's rho.

NOTE.—Schmitt 2-D Kaplan-Meier regression fits and errors from ASURV. The relations examined here are log $W_\lambda(line) \propto \log\ z$. Correlation probabilities in boldface meet our most stringent significance criteria: $P < 1\%$ in all 3 correlation tests using all data, and an upper limit fraction $< 33\%$.

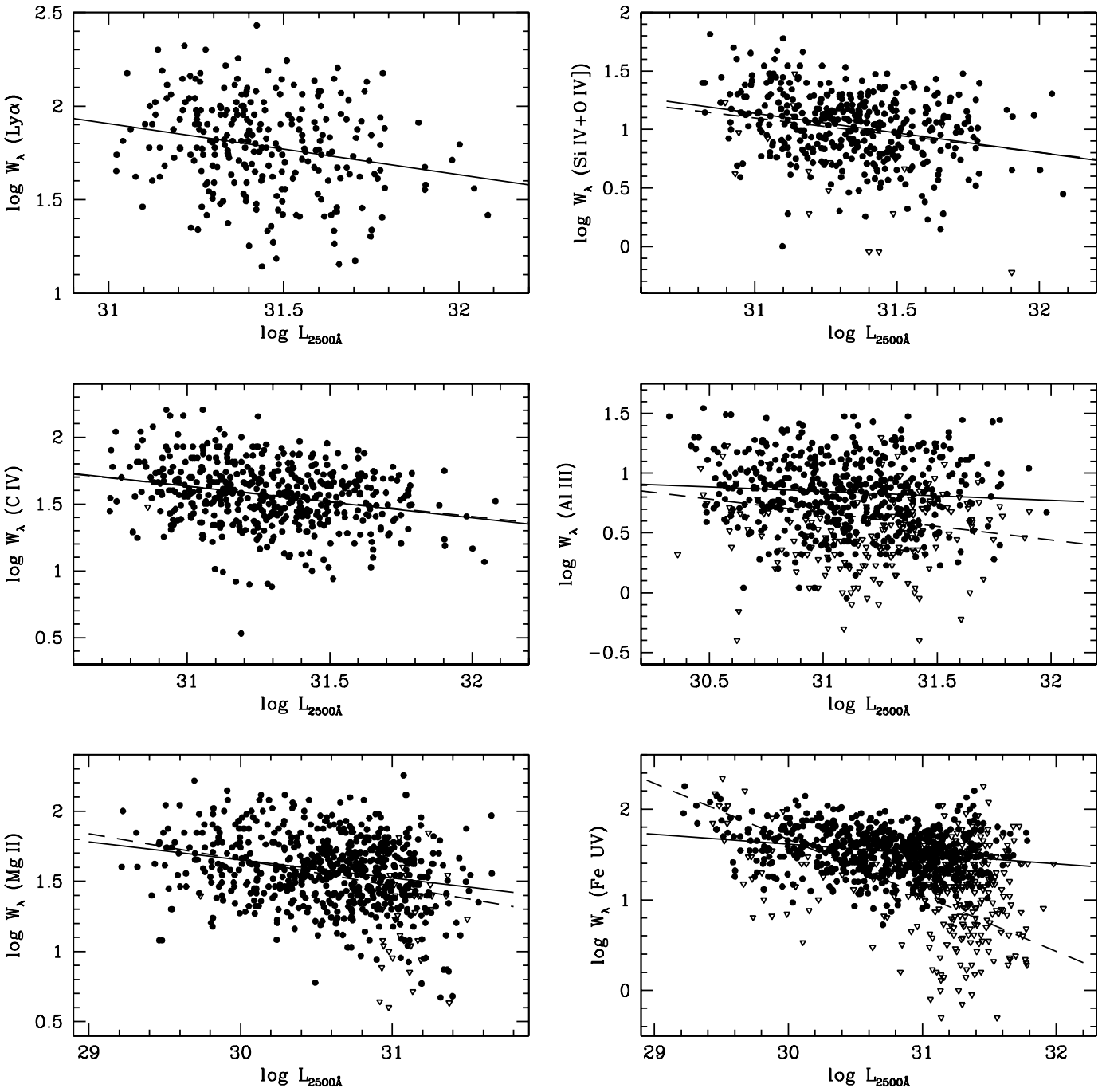

Fig. 1.— Significant log-log correlations between the emission line equivalent width and the monochromatic luminosity at 2500Å (in erg s^{-1} cm^{-2} Hz^{-1}) in the LBQS sample. Filled circles denote detections, open triangles upper limits in W_λ. Dashed lines are best-fit linear regression including upper limits. Solid lines show the best fit to detections only. In cases where there are few constraining upper limits, the two lines overlap.

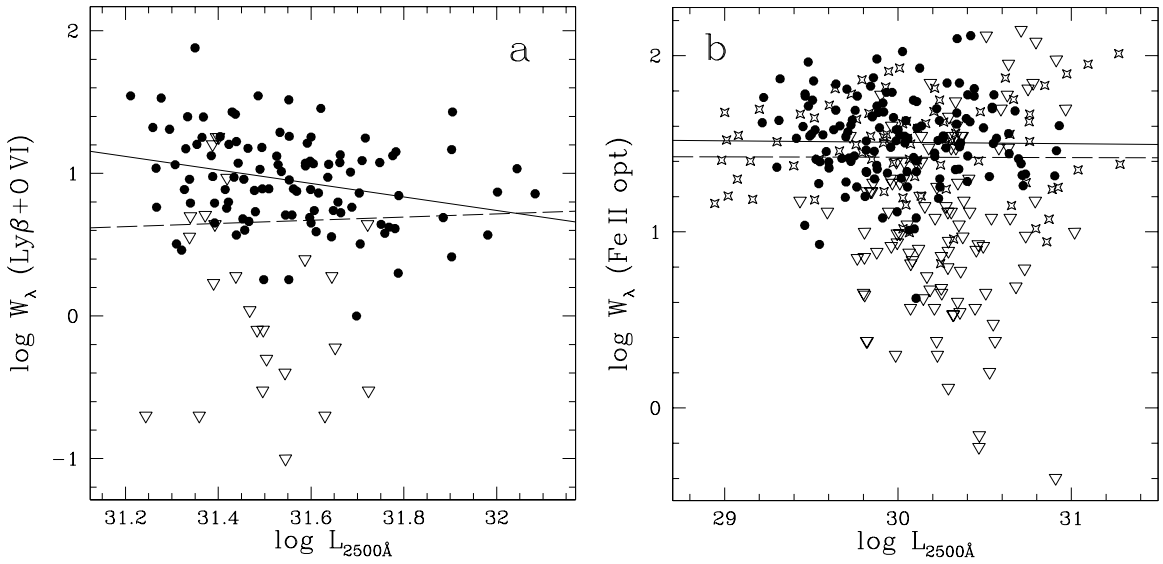

Fig. 2.— a) The relation between the O VI equivalent width and luminosity at 2500Å. No significant correlation is present. However when only detections are analyzed a significant correlation is found. The symbols have the same definition as in Figure 1. b) The correlation between the $FeII_{opt}$ equivalent width and luminosity at 2500Å for the LBQS and PG samples. Stars denote PG QSOs.

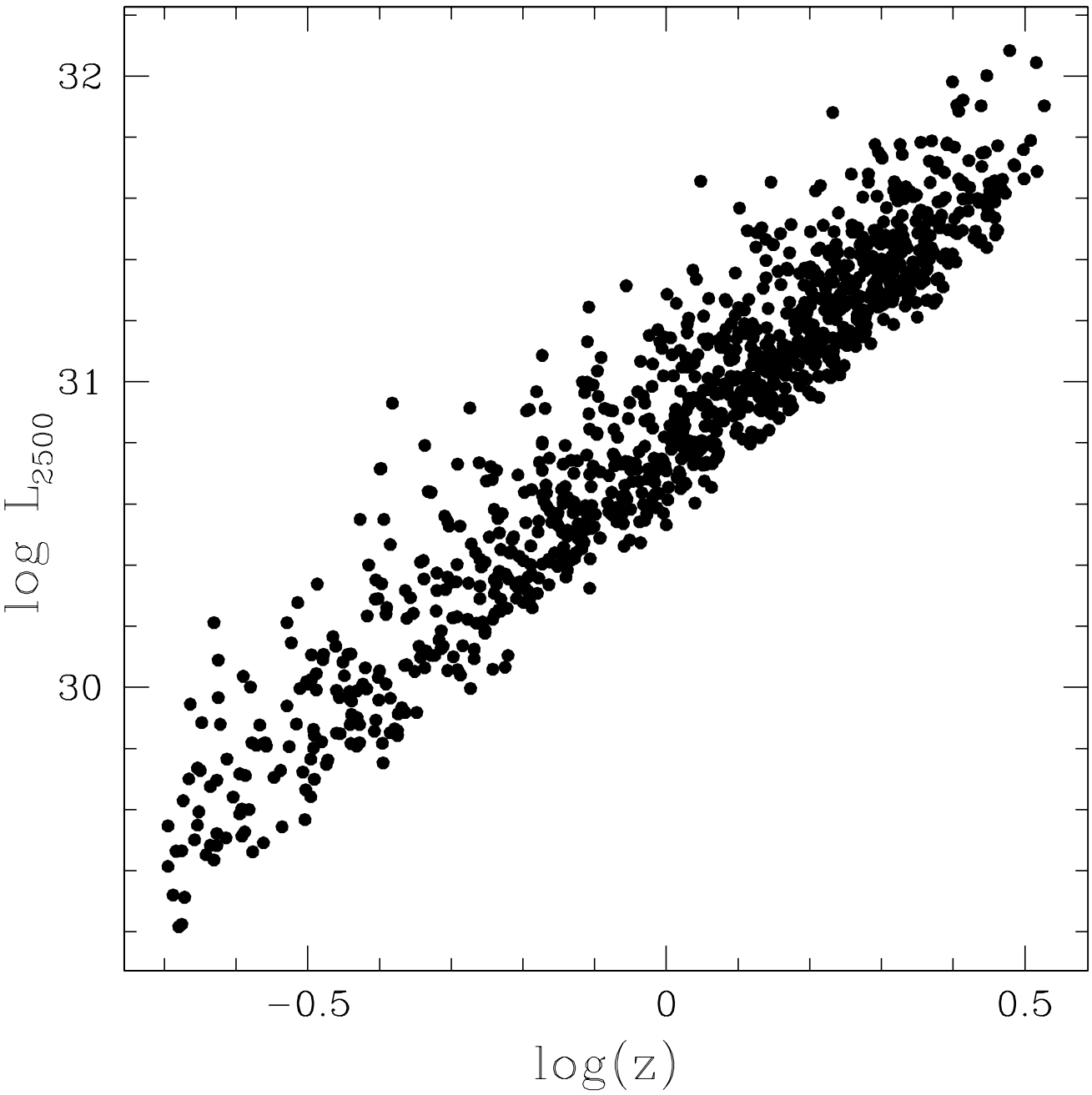

Fig. 3.— The logarithm of the monochromatic luminosity at 2500Å (in erg s^{-1} cm^{-2} Hz^{-1}) plotted against logarithm of the redshift z for QSOs in the LBQS sample. log L_{2500} is derived as decribed in § 2.

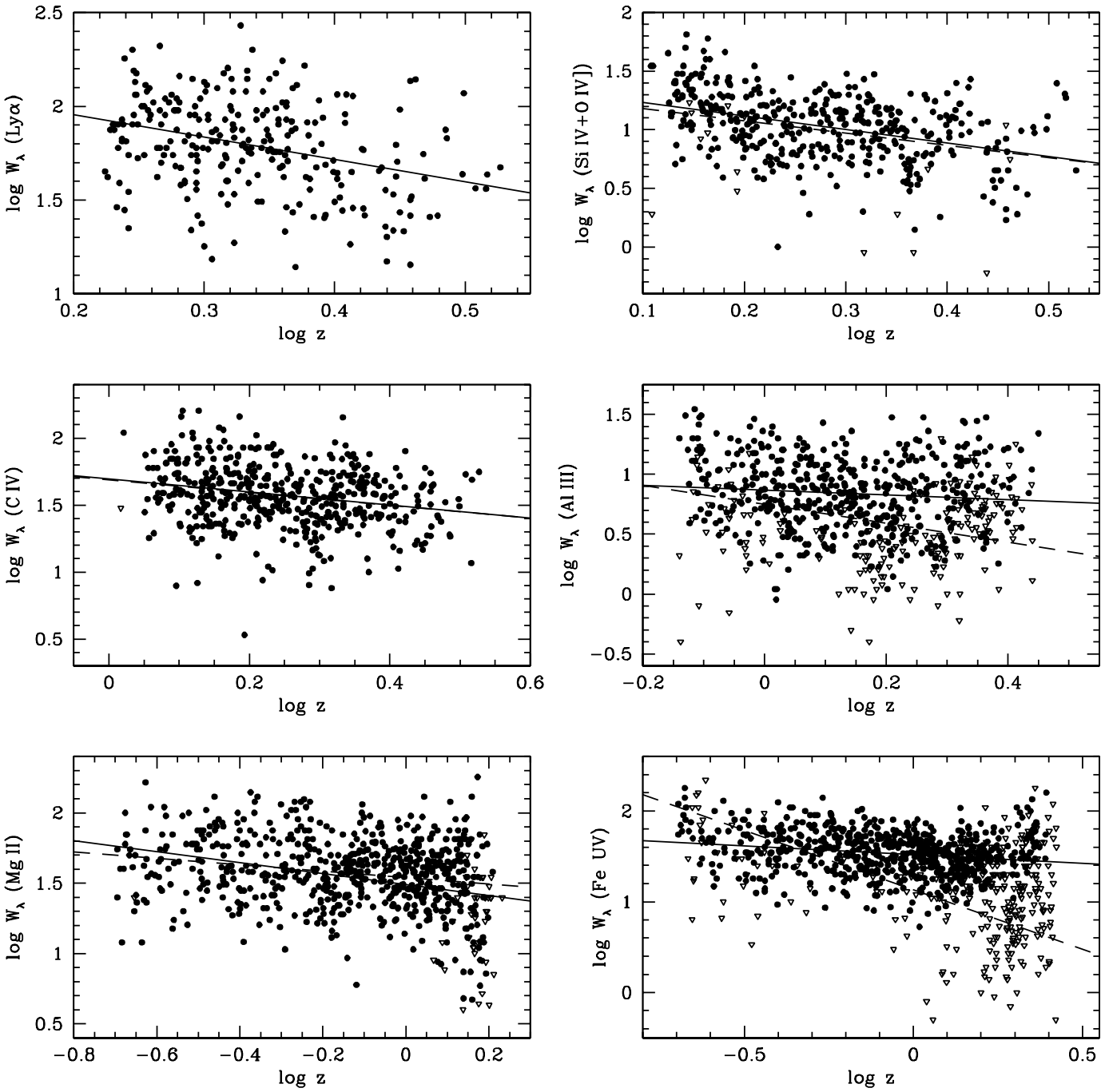

Fig. 4.— Significant log-log correlations between the emission line equivalent width and redshift in the LBQS sample. Symbols and regression lines have same meaning as in Figure 1. The dispersion in the panels is lower than in Figure 1, as reflected in the multivariate analysis results described in § 5 and Table 2.

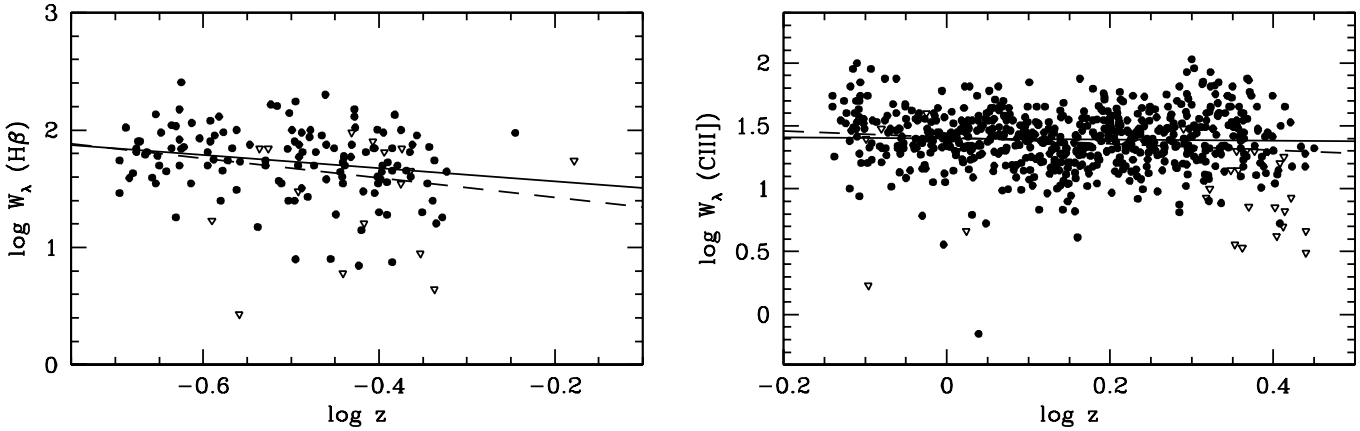

Fig. 5.— Significant log-log correlations between the emission line equivalent width and redshift in the LBQS sample for C III] and Hβ. Symbols and regression lines have same meaning as in Figure 1. These emission lines do not show a significant correlation with luminosity in the LBQS sample, or with redshift when detections alone are analyzed.

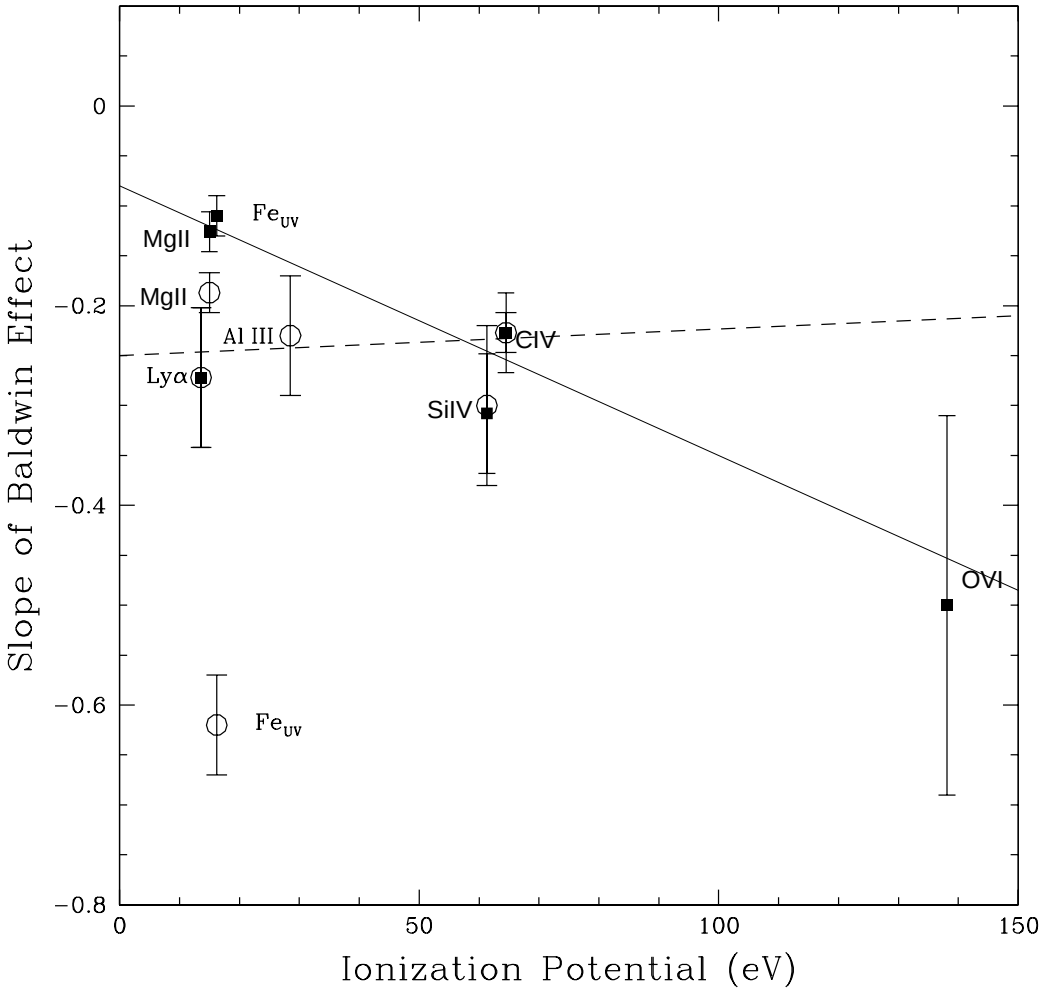

Fig. 6.— The slope of the Baldwin Effect as a function of ionization energy for line species with significant measured luminosity correlations. Open symbols (fit with the dashed line) represent the slopes of the Baldwin effect obtained from all data (including detections and upper limits). Solid symbols (fit with the solid line) represent the slope of the Baldwin effect for detections only. For the SiIV+OIV] blend, we use the mean of the ionization potentials for both ions. Statistically, the correlation is not significant, but any trend is heavily dependent on measurements of O VI.